Cell

Myosin VI Undergoes Cargo-Mediated Dimerization

Cong Yu,[1,3] Wei Feng,[1,3] Zhiyi Wei,[1] Yohei Miyanoiri,[1] Wenyu Wen,[1] Yanxiang Zhao,[2] and Mingjie Zhang[1,*]
[1]Department of Biochemistry, Molecular Neuroscience Center, Hong Kong University of Science and Technology, Clear Water Bay, Kowloon, Hong Kong
[2]Department of Applied Biology and Chemical Technology, Hong Kong Polytechnic University, Hung Hom, Kowloon, Hong Kong
[3]These authors contributed equally to this work
*Correspondence: mzhang@ust.hk
DOI 10.1016/j.cell.2009.05.030

SUMMARY

Myosin VI is the only known molecular motor that moves toward the minus ends of actin filaments; thus, it plays unique roles in diverse cellular processes. The processive walking of myosin VI on actin filaments requires dimerization of the motor, but the protein can also function as a nonprocessive monomer. The molecular mechanism governing the monomer-dimer conversion is not clear. We report the high-resolution NMR structure of the cargo-free myosin VI cargo-binding domain (CBD) and show that it is a stable monomer in solution. The myosin VI CBD binds to a fragment of the clathrin-coated vesicle adaptor Dab2 with a high affinity, and the X-ray structure of the myosin VI CBD in complex with Dab2 reveals that the motor undergoes a cargo-binding-mediated dimerization. The cargo-binding-induced dimerization may represent a general paradigm for the regulation of processivity for myosin VI as well as other myosins, including myosin VII and myosin X.

INTRODUCTION

Myosins are actin-based molecular motors that play vital roles in diverse cellular processes ranging from muscle contraction to intracellular transport (Foth et al., 2006; O'Connell et al., 2007; Sellers, 2000). Myosin VI is the only known motor that transports cargoes to the minus ends of the actin filaments (Mermall et al., 1994; Wells et al., 1999). Originally discovered as an F-actin-binding protein in *Drosophila*, myosin VI has subsequently been identified in many other species (Baker and Titus, 1997; Hasson and Mooseker, 1994; Hasson et al., 1996; Kellerman and Miller, 1992). Myosin VI-mediated cargo transport is essential for a host of cellular processes, including clathrin-dependent endocytosis, the maintenance of the *cis*- and *trans*-Golgi network and exocytosis at the Golgi complexes, and the asymmetric distribution of cellular components in polarized cells (see reviews, Buss and Kendrick-Jones, 2008; Buss et al., 2004; Sweeney and Houdusse, 2007). In addition to its transporting roles, myosin VI also serves as an anchor that supports cellular architectures by physically connecting cytoskeletons with its binding targets, such as membranes. As an anchor, myosin VI is indispensable for the development and maintenance of highly organized cellular structures, such as the stereocilia of hair cells in ears (Hasson et al., 1997; Seiler et al., 2004), the leading edges of migrating cells (Geisbrecht and Montell, 2002), and the establishment and maintenance of the apicobasal polarity of epithelia (Maddugoda et al., 2007). In addition to myosin VI, other unconventional myosins (e.g., myosin VII, myosin X, and myosin XV) can also function both as transporters and as anchors (Knight et al., 2005; Yang et al., 2006). However, the molecular mechanisms dictating this functional dichotomy of the unconventional myosins are largely unknown.

Myosin VI contains an N-terminal motor domain followed by a short neck (also called the lever arm), a hypothetical coiled-coil domain in the middle, and a C-terminal globular cargo-binding domain (CBD) (Figure 1A). Recent structural and biochemical studies of the motor domain have revealed that a unique insertion between the motor domain and the neck region confers the reverse moving directionality to myosin VI (Bryant et al., 2007; Menetrey et al., 2005). The structural rearrangement of this insertion, together with the neck, also provides a partial explanation for the large power-stroke of myosin VI (Menetrey et al., 2007, 2008). Recent studies of the putative coiled-coil region indicate that it forms an extended monomeric helix instead of the previously expected dimeric coiled-coil (Rock et al., 2001; Spink et al., 2008). This finding provides a plausible explanation for the unexpectedly large step size (~36 nm) of myosin VI but also raises an important question concerning the dimerization mechanism of the motor.

The C-terminal CBD of myosin VI recognizes and selects its binding cargoes (Buss et al., 2004; Sweeney and Houdusse, 2007). Several adaptor proteins have been reported to interact specifically with the CBD, thus defining the specific subcellular functions of myosin VI: an endocytic adaptor protein Disabled-2 (Dab2), which links myosin VI to clathrin-coated vesicles at the early stages of endocytosis (Buss et al., 2001; Inoue et al., 2002; Morris et al., 2002); GIPC, another endocytic adaptor, which bridges myosin VI to the clathrin-uncoated vesicles for the late stages of endocytosis (Aschenbrenner et al., 2003; Bunn et al., 1999; Naccache et al., 2006; Reed et al., 2005); and a Golgi resident adaptor optineurin, which provides a linkage between myosin VI and the Golgi complex during biosynthetic exocytosis (Au et al., 2007; Sahlender et al., 2005). In addition to cargo recognition, the myosin VI CBD has recently been

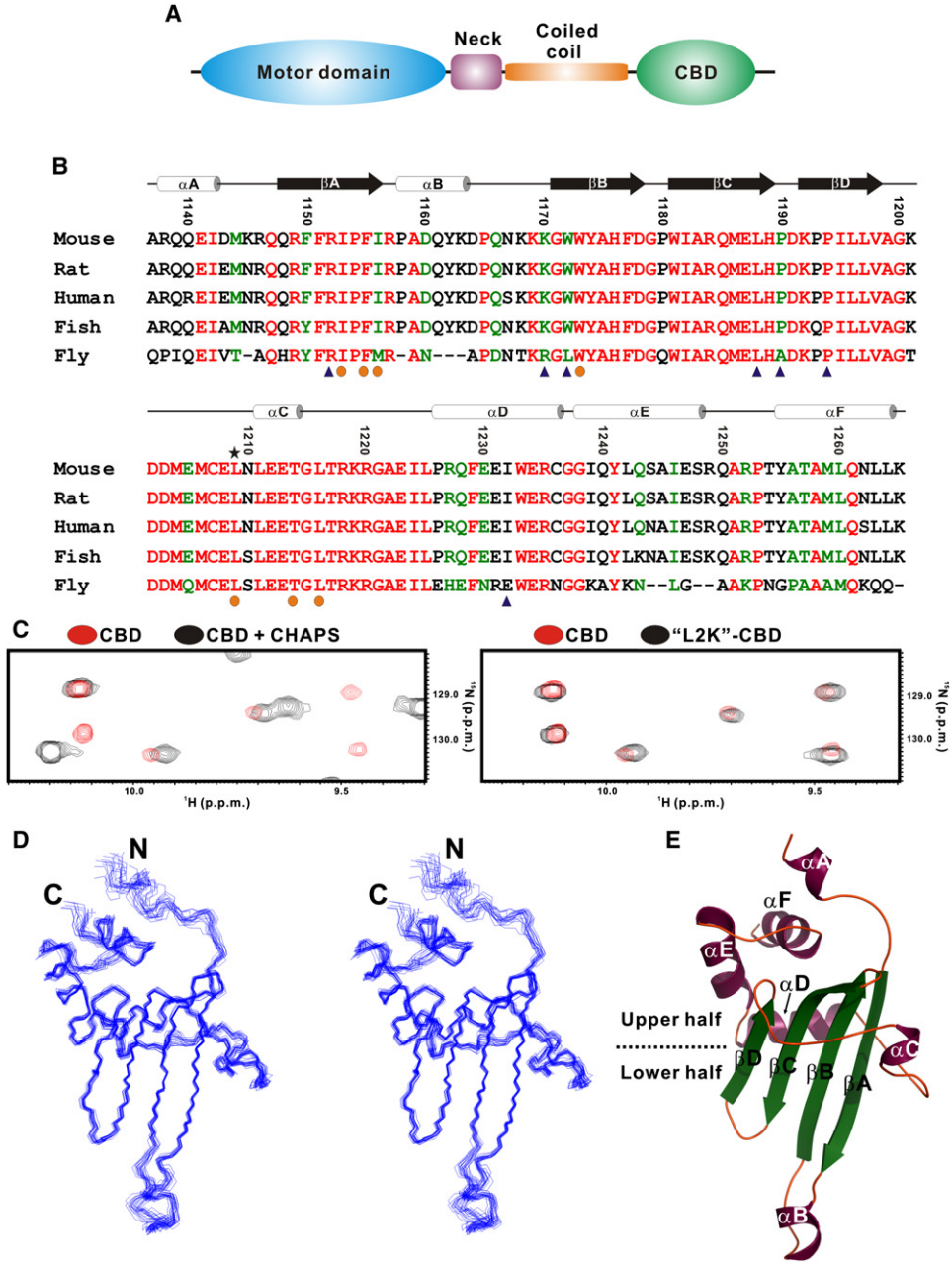

Figure 1. Structure of the Apo-Myosin VI CBD

(A) Schematic diagram showing the domain organization of myosin VI.

(B) Amino acid sequence alignment of the CBD from various species of myosin VI. In this alignment, the completely and highly conserved residues are shown in red and green, respectively. The secondary structure derived from the NMR structure of the domain is indicated in the alignment. The residues forming the binding sites I and II for Dab2 are highlighted with dots and triangles underneath the sequences, respectively. Leu1209, which was substituted with Lys for the structure determination of the apo-CDB, is indicated with an asterisk at the top of the alignment.

(C, left) An overlay plot of a selected region of the ^{1}H-^{15}N HSQC spectrum of the wild-type myosin VI CBD without and with the addition of 0.5% CHAPS in the sample buffer, showing significant chemical shift differences of the domain induced by the binding of CHAPS. (C, right) An overlay plot of the same region HSQC spectrum of the wild-type CBD with that of the L1209K-CBD, showing that the mutation does not alter the conformation of the domain.

(D) Stereo view showing the overlay of the backbones of the final 20 NMR structures of myosin VI L2K-CBD.

(E) Ribbon diagram representation of the apo-myosin VI CBD.

shown to be involved in the dimerization of myosin VI (Spudich et al., 2007). Electron microscopy (EM) studies of myosin VI in vitro showed that purified myosin VI can form dimers at high concentrations, and this clustering-induced dimerization is somewhat inhibited by its CBD (Park et al., 2006). In contrast, a fluorescence resonance energy transfer-based assay in vivo

demonstrated that myosin VI forms dimers on the surface of transport vesicles in a CBD-dependent manner (Altman et al., 2007). Myosin VI needs to form a processive dimer for its transport function (Altman et al., 2007; Park et al., 2006; Spink et al., 2008). Intriguingly, it has been shown that purified native myosin VI exists as a nonprocessive monomer in solution (Lister et al., 2004), and the monomeric myosin VI has been proposed to function mainly as an anchor (Buss et al., 2004). Therefore, the elucidation of the molecular mechanism governing the monomer-dimer conversion of myosin VI represents a task crucial to understanding the cellular functions of myosin VI as well as other unconventional myosins.

Here, we describe our 8 year journey in the elucidation of the myosin VI cargo recognition mechanism. The solution structure of the monomeric apo-myosin VI CBD solved in this work reveals that myosin VI exists as a stable monomer in the absence of cargoes. The crystal structure of the myosin VI CBD/Dab2 complex shows that the myosin VI CBD forms a cargo-induced dimer, suggesting that the motor undergoes a cargo binding-dependent monomer-to-dimer conversion. This cargo binding-mediated monomer-to-dimer conversion mechanism adopted by myosin VI may be shared by other unconventional myosins, such as myosin VII and myosin X.

RESULTS

Structural Determination of the Apo-Form Myosin VI CBD

We initiated biochemical and structural characterizations of the myosin CBD when this domain was implicated in cargo selections (Inoue et al., 2002; Morris et al., 2002; Wu et al., 2002). The entire myosin VI CBD contains ~200 residues, and the N-terminal 1/3 of this 200 residue fragment was shown to bind to lipid membranes and cargoes such as GIPC and optineurin (Reed et al., 2005; Sahlender et al., 2005; Spudich et al., 2007). The myosin VI CBD studied in detail here corresponds to the C-terminal ~2/3 of the entire tail domain (residues 1137–1265). Amino acid sequence alignment analysis showed that the myosin VI CBD is highly conserved throughout its evolution, with no recognizable protein domains known to date and no homologous sequences in other proteins (Figure 1B). Our initial biochemical analysis showed that the myosin VI CBD forms a stable monomer at low concentrations (<0.2 mM) in solution, with a well-folded tertiary structure as indicated by the well-dispersed NMR spectrum of the domain (Figure S1A available online). Unfortunately, the NMR spectra of the CBD deteriorated progressively with the increase of its concentration due to nonspecific sample aggregation (Figure S1B). Extensive efforts in trying to obtain crystals of the CBD were not successful. Systematic NMR-based sample condition screenings with various buffers, salts, and additives revealed that the inclusion of 0.5%–1% CHAPS in the sample buffer significantly improved the quality of the CBD spectra (Figure S1C), suggesting that the domain tends to aggregate via hydrophobic interactions at elevated concentrations. Due to technical difficulties, we were only able to determine the solution structure of the myosin VI CBD in the presence of CHAPS by NMR spectroscopy at a low resolution (data not shown). Nevertheless, this low-resolution structure served as a template for us to design strategies for obtaining the high-resolution structure of the domain. Additionally, the large chemical shift changes of the CBD induced by CHAPS binding indicated that the CBD structure determined in the presence of CHAPS may not represent its bona fide structure in its apo-form (Figures 1C and S2A). Guided by the solution structure of the CBD in the presence of CHAPS and aided by the NMR-based sample condition screenings, we tested a large number of point mutations of the CBD in an attempt to disrupt the concentration-dependent aggregation observed in the wild-type protein. One of the mutants tested, with Leu1209 substituted with Lys (denoted as "L2K"-CBD), displayed an excellent NMR spectrum even at a concentration of ~1 mM (Figure S1D). Importantly, the spectrum of the L2K-CBD overlaps very well with that of the wild-type protein except for a few residues surrounding Leu1209, indicating that the substitution of Leu1209 with Lys did not introduce significant changes to the structure of the myosin VI CBD (Figures 1C and S2B).

We next determined the high-resolution structure of L2K-CBD using NMR spectroscopy. The overall structure of the CBD is well defined except for the N and C termini and the loop between the first and the second β strands (Figure 1D and Table S1). The myosin VI CBD contains four β strands (βA–βD) and six α helices (αA–αF). The four β strands form an antiparallel β sheet, which forms the core of the domain. One side of the β sheet is covered by three helices (αD–αF), which pack with each other perpendicularly; the other side of the sheet is largely exposed to the solvent with a short αC helix capped at one of its edges (Figure 1E). No folds similar to the myosin VI CBD were found in the Protein Data Bank (PDB) when searching with the Dali algorithm (http://www.ebi.ac.uk/dali/). Interestingly, the packing between the helices (αC and αD–αF) and the β sheet is limited to one end (arbitrarily referred to as the up-half) of the β sheet, leaving the lower half of the β sheet completely exposed (Figures 1E and S3). A short and somewhat mobile helix (αB) connects the βA and βB strands at the extreme end of the lower half of the CBD β sheet (Figures 1D and 1E). Analysis of the surface properties of the myosin VI CBD showed that the domain contains a prominent hydrophobic surface located at one face of the lower half of the β sheet (Figures 1E and S3). This hydrophobic surface is responsible for the concentration-dependent aggregation of the wild-type CBD. The structure also explains why the L2K mutation significantly weakens such hydrophobic interactions without altering the overall structure of myosin VI CDB (Figures S3A and S3B). This L2K mutation has been extremely valuable in the structure determination of the apo-form myosin VI CBD. However, the caveat of the mutation is that it essentially prevented the CBD from binding to its targets (see below for details).

Dab2 Binds to the Myosin VI CBD via an Extended Region within Its C-Terminal Tail

The best known myosin VI CBD-binding partner known to date is Disabled-2 (Dab2) (Inoue et al., 2002; Mishra et al., 2002; Morris et al., 2002; Morris and Cooper, 2001). In view of the critical role of the myosin VI/Dab2 interaction in clathrin-coated vesicle-mediated endocytosis(Mishra et al., 2002; Morris et al., 2002), we decided to characterize this interaction in detail. Dab2 is composed of an N-terminal PTB domain and a long C-terminal

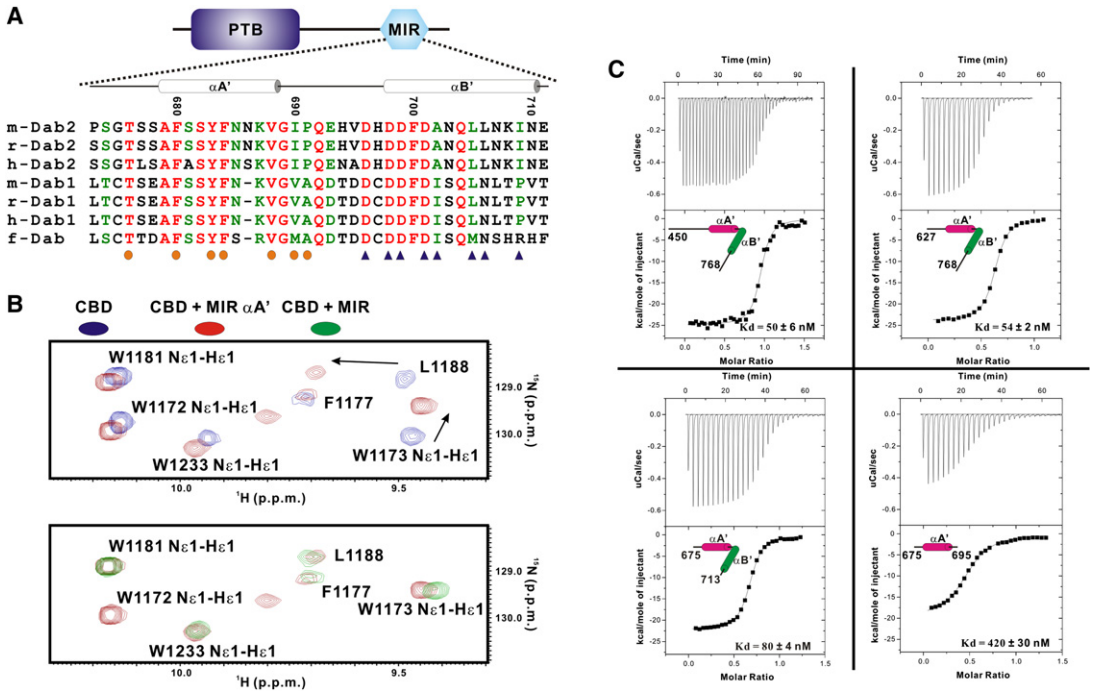

Figure 2. The Myosin VI CBD Binds to an Extended Fragment of Dab2 with High Affinity

(A) Amino acid sequence alignment of the Dab2 myosin VI interaction region (MIR) with the same color coding as in Figure 1B. The two α helices of the Dab2 MIR are indicated. The Dab2 MIR residues interacting with the residues from sites I and II of the myosin VI CBD are highlighted with dots and triangles underneath the sequences, respectively.

(B, top) An overlay plot of a selected region of the ^{1}H-^{15}N HSQC spectrum of the apo-myosin VI CBD and the domain saturated with the N-terminal half of the MIR fragment containing only the αA′ helix (residues 675–695), showing significant chemical shift changes of the myosin CBD induced by the N-half MIR peptide binding. (B, bottom) An overlay plot of the same region of HSQC spectra of the CBD bound to the N-half and the complete Dab2 MIR fragments, showing that inclusion of the αB′ helix of the Dab2 MIR induces additional chemical shift changes to the myosin VI CBD.

(C) ITC-based measurements of the bindings of various Dab2 fragments to the wild-type myosin VI CBD. The details of the Dab2 MIR fragments used in the binding assay and the fitted dissociation constants with standard errors are indicated in each panel.

tail with no recognizable domains (Figure 2A). Dab2 has been shown to bind to myosin VI via its C-terminal tail. It was shown that substitution of the "^{682}SYF^{684}"-motif within this Dab2 C-terminal tail with an "AAA" cassette abolished Dab2's binding to the GST-fused CBD of myosin VI (Morris et al., 2002). We confirmed the direct interaction between the myosin VI CBD and the entire C-terminal tail of the wild-type Dab2 and verified that the ^{682}SYF^{684}-motif of Dab2 is absolutely required for binding to myosin VI (data not shown). A 21 residue synthetic peptide comprising residues 675–695 of Dab2 was used for detailed characterization of the interaction between Dab2 and myosin VI. The boundaries of the Dab2 peptide were chosen based on the following findings: further extension to the N-terminal end beyond residue 675 did not further increase the binding affinity of Dab2 to myosin VI (data not shown), and the C-terminal end was chosen because it was shown that the "^{699}DFD^{701}"-motif of Dab2 was not required for myosin VI binding (Morris et al., 2002). NMR-based titration experiments showed that the Dab2 peptide indeed binds to the myosin VI CBD with a 1:1 stoichiometry. An ITC-based assay showed that the 21 residue Dab2 peptide binds to the myosin VI CBD with a dissociation constant (K_D) of ~0.5 μM (Figure 2C). We believed that this 21 residue peptide most likely represented the complete myosin VI-binding domain of Dab2, and we used NMR and X-ray methods to try to determine the structure of the myosin VI CBD in complex with this 21 residue peptide. However, we were never able to prepare a wild-type CBD/Dab2 peptide complex that was suitable for NMR-based structure determination. Extensive screening for crystals of the complex also failed.

We decided to revisit the interaction between the myosin VI CBD and Dab2 using longer fragments of Dab2. Powered by the exquisite sensitivity of NMR chemical shifts in response to target bindings, we discovered that addition of a Dab2 fragment with a C-terminal extension covering the ^{699}DFD^{701}-motif (residues 675–713) induced additional chemical shift changes to a number of residues in the myosin VI CBD (Figure 2B, bottom panel and Figure S4), indicating that the ^{699}DFD^{701}-motif, previously identified to be dispensable for myosin VI binding (Morris et al., 2002), is actively involved in the Dab2/myosin VI interaction. Detailed chemical shift perturbation analysis showed that the binding of the 21 residue Dab2 peptide induced chemical shift changes limited to one side of the CBD β sheet. This 21 residue Dab2 binding side of the myosin VI CBD β sheet (referred to as "site I," Figures S4A and S4B) is highly hydrophobic (Figure S3B) and complements the hydrophobic nature of the N-terminal half of the longer Dab2 fragment (Figure 2A).

Table 1. Statistics of Data Collection and Model Refinement of the Myosin VI CBD/Dab2 MIR Complex

Data Collection			
Data Sets	Native	NaI	
Space group	$P2_1$	$P2_1$	
Unit cell parameters (Å)	a = 69.2, b = 70.0, c = 78.5 β = 98.0	a = 69.2, b = 70.0, c = 78.5 β = 98.3	
Resolution range (Å)	30–2.2 (2.32–2.2)	30–2.6 (2.74–2.6)	
No. of total reflections	135314 (18948)	183092 (26377)	
No. of unique reflections	36631 (5217)	23184 (3348)	
I/σ	14.6 (2.3)	16.0 (2.6)	
Completeness (%)	97.0 (95.3)	99.9 (100.0)	
R_{merge} (%)[a]	8.4 (54.8)	15.2 (70.3)	
Structure Refinement			
Resolution (Å)	30–2.2 (2.257–2.2)		
R_{cryst}/R_{free} (%)[b]	18.9 (25.0)/25.1 (31.9)	rmsd bonds (Å)/angles (°)	0.009/1.09
No. of reflections		No. of atoms	
working set	34798	protein atoms	5108
test set	1833	water molecules	266
Average B factor (Å^2)		Ramachandran plot	
main chain	31.2	most favored regions (%)	96.2
side chain	32.7	additionally allowed (%)	3.8
water	30.1	generously allowed (%)	0.0

Numbers in parentheses represent the value for the highest resolution shell.
$R_{free} = \Sigma_T||F_{obs}| - |F_{calc}||/\Sigma_T|F_{obs}|$, where T is a test data set of about 5% of the total reflections randomly chosen and set aside prior to refinement.
[a] $R_{merge} = \sum|I_i - I_m|/\sum I_i$, where I_i is the intensity of the measured reflection and I_m is the mean intensity of all symmetry-related reflections.
[b] $R_{cryst} = \Sigma||F_{obs}| - |F_{calc}||/\Sigma|F_{obs}|$, where F_{obs} and F_{calc} are observed and calculated structure factors.

Extending the Dab2 peptide to cover the ^{699}DFD^{701}-motif (residues 675–713) induced additional chemical shift changes to the residues located at the opposite side of the myosin VI CBD β sheet (referred to as "site II," Figures S4C and S4D), which is rich in positively charged residues (Figure S3B) and matches well with a cluster of the negatively charged residues at the C-terminal half of the longer Dab2 fragment (Figure 2A). Taken together, the above biochemical and spectroscopic studies reveal that the myosin VI CBD contains two discrete Dab2-binding sites located at the two sides of the myosin VI CBD β sheet (Figure S4), and that a 39 residue fragment of Dab2 is directly involved in myosin VI binding. The binding affinity of this 39 residue extended Dab2 fragment to the myosin VI CBD (K_D ~80 nM) is about five times higher than the 21 residue Dab2 peptide (Figure 2C). Further extension at the C-terminal end of this 39 residue Dab2 fragment did not increase its binding affinity to the myosin VI CBD (Figure 2C), indicating that this 39 residue Dab2 fragment (instead of the 21 residue Dab2 peptide selected initially) represents the complete myosin VI-binding region of Dab2. We referred to this myosin VI-interacting region as MIR (*m*yosin VI *i*nteraction *r*egion, Figure 2A). It is noted that the Dab2 MIR sequence is also found in Dab1; this explains why myosin VI also binds to Dab1 (Morris et al., 2002). Additionally, the MIR sequence is highly conserved within the Dab family proteins throughout their evolution, indicating that the myosin VI/Dab2 interaction (hence myosin VI-mediated endocytosis) characterized here is a conserved molecular process throughout the evolution.

Dab2 Binding-Mediated Dimerization of Myosin VI

We next wanted to determine, by either NMR or X-ray methods, the structure of myosin VI in complex with the complete Dab2 MIR. Obviously, we needed to use the wild-type myosin VI CBD instead of its L2K mutant to prepare the complex. However, the concentration-dependent aggregation of the wild-type myosin VI CBD prevented us from making stable and homogeneous complex samples (as indicated by the ^{1}H-^{15}N HSQC spectra of the complex) by either mixing it with the Dab2 MIR or coexpressing the two proteins in bacteria. Extensive attempts to grow crystals of the myosin VI CBD/Dab2 MIR complexes using the mixed or coexpressed samples were not successful either, likely due to the sample heterogeneity. To overcome the above problem, we fused the Dab2 MIR peptide to either the N- or the C-terminal end of the myosin VI CBD, hoping that the fused proteins would be strictly 1:1 stoichiometric between the CBD and the MIR. One of the myosin VI-Dab2 fusion proteins with the MIR peptide fused to the C terminus of the CBD using a 15 residue Gly-Ser flexible linker together with a thrombin cleavage sequence in the middle was highly soluble and stable. The single chain fusion protein was, however, heterogeneous in its conformation as indicated by its NMR spectrum (Figure S5A). The NMR spectrum of the fusion protein after thrombin cleavage was highly homogenous and well dispersed at protein concentrations up to ~1.5 mM (Figure S5B), indicating that a homogenous and stoichiometric myosin VI CBD/Dab2 MIR complex was successfully prepared using this approach. High-quality crystals (Table 1) of the myosin VI CBD/Dab2 MIR complex

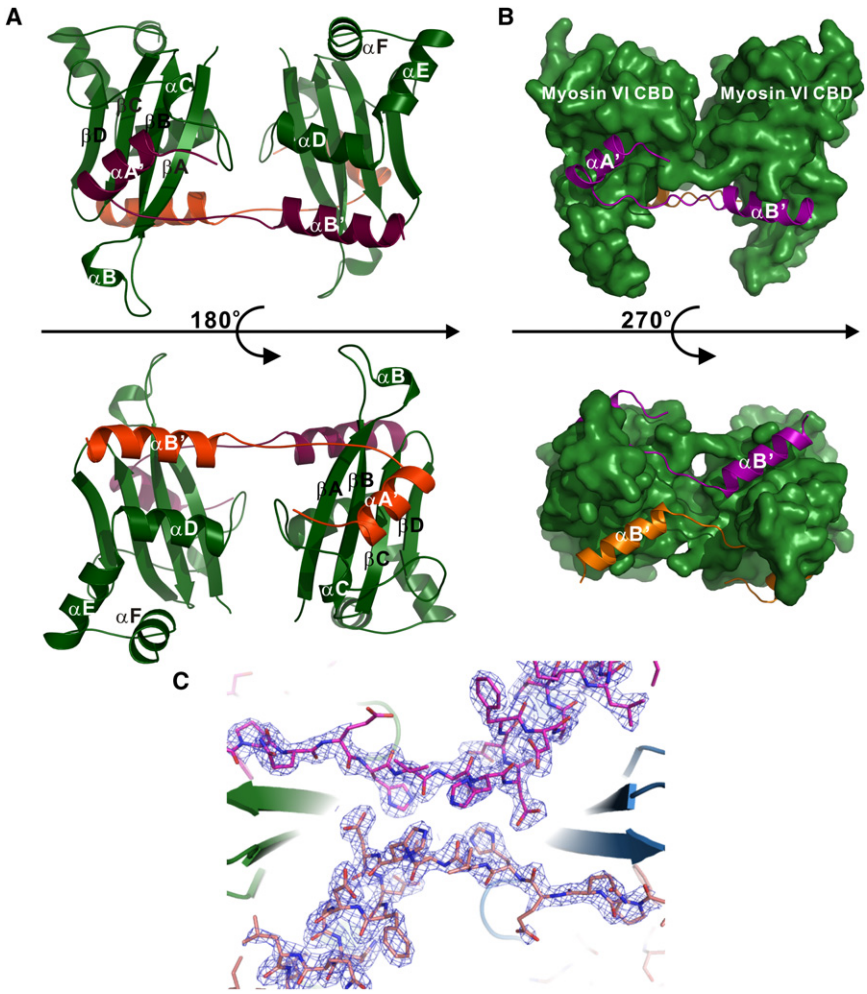

Figure 3. The Overall Structure of the Myosin VI CBD/Dab2 MIR Complex

(A) Ribbon diagram representations showing the Dab2 MIR-induced dimerization of the myosin VI CBD. In this diagram, the myosin CBD is drawn in green and two Dab2 MIR fragments are colored in purple and orange.

(B) Surface diagram showing the binding surface of the Dab2 MIR on the myosin VI CBD.

(C) The electron density map of the Dab2 MIR in the myosin VI CBD/Dab2 MIR complex. The green and blue ribbons are partial β strands from the myosin CBD in the complex.

were readily obtained in several crystallization buffer conditions using the complex sample prepared as described above.

The structure of the myosin VI CBD/Dab2 MIR complex was determined by preparing iodine derivatives of the complex crystals (Table 1). The most striking finding of the myosin VI CBD/Dab2 MIR complex is that the myosin VI CBD forms a symmetric dimer that is tethered by two molecules of the Dab2 MIR (Figures 3A and 3B). In the complex, the myosin VI CBD adopts a similar conformation to the apo-form protein, except that the flexible N-terminal helix (αA) is missing in the complex. The Dab2 MIR forms two helices (αA′ and αB′), corresponding to the N-terminal and C-terminal halves of the MIR (Figures 2A and 3A). The N-terminal helix (αA′) of the Dab2 MIR binds to site I of one molecule of the myosin VI CBD, and the C-terminal helix (αB′) of the same Dab2 MIR binds to site II of the other CBD in the complex. The two CBD molecules in the myosin VI/Dab2 complex do not physically contact each other. Therefore, the formation of the myosin VI dimer in the complex is exclusively induced by the binding of Dab2. The high-quality electron density map at the crossover points of the two Dab2 MIR molecules excluded the possibility of mis-tracing the Dab2 MIR chains (Figure 3C). The myosin VI/Dab2 complex structure solved here provides a definitive picture showing the cargo binding-mediated dimerization of myosin VI.

We verified that the dimeric myosin VI CBD/Dab2 complex observed in the crystal structure also exists in solution. The myosin VI CBD/Dab2 complex interacted nonspecifically with beads in gel filtration columns (i.e., analytical gel filtration cannot be used to assess the molecular mass of the complex; data not shown). As an alternative approach, we used a site-specific chemical crosslinking approach to probe the dimer state of the complex. The structure of the dimeric myosin VI CBD/Dab2 MIR complex shows that L1225 in the αC/αD loop of the CBD represents the closest neighboring residues of the two noncontacting CBD molecules in the complex (a distance of ~4.4 Å between Cγ of the two Leu residues) (Figures 3 and 4A). We reasoned that the substitution of L1225 with Cys would specifically promote the formation of the disulfide bond-mediated CBD dimer of the CBD/MIR complex, as the distance of the two Cys side chains in the complex is nearly ideal for spontaneous disulfide bond formation. In contrast, neither the apo-CBD nor the CBD in complex with the short Dab2 MIR containing only αA′ would form specific disulfide-mediated CBD dimers with the same L1225C mutation. Exactly as we have predicted, no CBD dimer could be observed in the nonreducing SDS-PAGE for the apo-CDB(L1225C) and CDB(L1225C) saturated with the short Dab2 MIR peptide containing only αA′. In contrast, CBD(L1225C) was found to form a quantitative dimer in complex with the longer form of the Dab2 MIR, with or without the addition of the dimer-promoting catalyst $[Cu(Phen)_3]^{2+}$ (Figure 4B). The addition of DTT completely disrupted this disulfide-mediated covalent dimer of the myosin VI CBD as observed on the SDS-PAGE. Therefore, we conclude that the dimeric myosin VI CBD/Dab2 MIR complex structure revealed in the crystal structure also exists in solution. The second helix (αB′) of the Dab2 MIR is absolutely required for the Dab2-mediated dimerization of the myosin VI CBD.

Interface between the Myosin VI CBD and the Dab2 MIR

As revealed by both our NMR and X-ray crystallographic studies, the myosin VI CBD contains two discrete Dab2-binding sites,

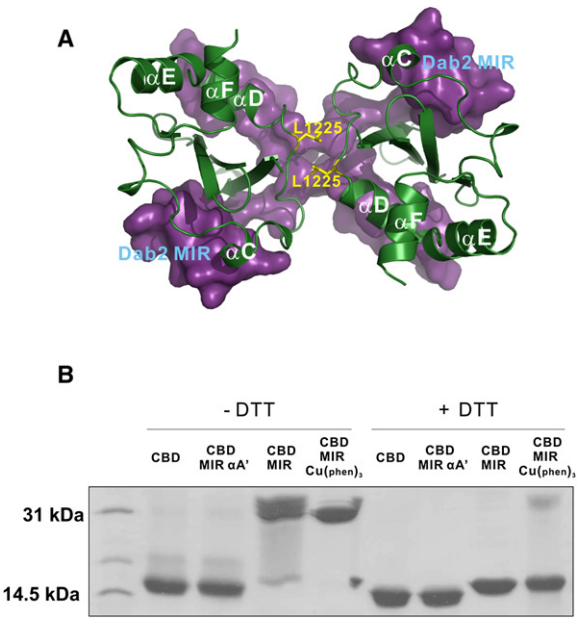

Figure 4. Dab2 MIR Binding-Induced Dimerization of Myosin VI in Solution

(A) Combined ribbon (myosin VI CBD) and surface (Dab2 MIR) representation of the mysoin VI/Dab2 complex. The side chains of Leu1225 immediately N-terminal to αD (shown in the explicit atomic model) are the closest residues of the two myosin CBD molecules in the complex. Leu1225 was substituted with Cys for disulfide-mediated crosslinking experiments in probing the dimer structure of the myosin VI CBD in the complex.

(B) Disulfide-mediated formation of the covalent myosin VI CBD dimer requires binding of the entire Dab2 MIR fragment containing both αA′ and αB′ helices. Neither apo-CBD nor CBD saturated with the N-half of the Dab2 MIR containing only αA′ (MIR αA′) could form a disulfide-mediated dimer, as assessed by nonreducing SDS-PAGE. The figure also showed that inclusion of the disulfide bond-promoting reagent, $[Cu(phen)_3]SO_4$, converted the CBD into a quantitative dimer when the domain was saturated with the Dab2 MIR. Finally, the disulfide-mediated the myosin VI CBD dimer induced by the binding of the Dab2 MIR can be completely reversed by the addition of an excess amount of DTT in the SDS-PAGE sample buffer. The gel was stained with Coomassie blue dye. The slightly lager CBD mass shown in the complex with the MIR is due to extra residues carried over after cleavage of the CBD-MIR fusion protein by thrombin.

namely, site I and site II (Figure 5). Site I is mainly formed by hydrophobic residues from βA, βB, and αC of the myosin VI CBD, which are located at one face of the CBD β sheet, and accommodates αA′ of the Dab2 MIR chiefly via hydrophobic interactions (Figures 5A and 5B). The side chains of F680, Y683, F684, and V688 (the "FxxYF"-motif in αA′) of the Dab2 MIR contact extensively with I1153, F1155, W1173, L1209, T1214, and L1216 in site I of the myosin VI CBD (Figures 5A and 5B). In addition, the backbones of I690 and P691 of the Dab2 MIR form a mini-antiparallel β sheet with the C-terminal end of the CBD βA. The side chains of I690 and P691 of the MIR interact with the side chains of I1156 and F1155 from the CBD, respectively. The single point mutation in site I (L1209 to K, the mutant used for the structural determination of the apo-myosin VI CBD) dramatically decreased its Dab2 binding (Figure 5D), indicating that the interaction in site I plays a dominant role in myosin VI/Dab2 binding. Site II is at the opposite face of the CBD β sheet with respect to site I, and the residues in site II bind to αB′ of the Dab2 MIR via both charge-charge and hydrophobic interactions (Figures 5A and 5C). The positively charged R1152 and K1170 from the myosin VI CBD form a charge-charge interaction network with D696, D698, D699, and D701 from the Dab2 MIR. The Nε1 of W1172 from the CBD forms a hydrogen bond with the carboxyl oxygen of D698 (Figure 5C). The side chains of A702, L705, L706, and I709 of the Dab2 MIR interact with the hydrophobic side chains of W1172, L1188, P1190, P1194, and I1232 from the myosin VI CBD. Interestingly, the substitution of R1152 of the CBD with Glu (referred to as the "R2E" mutant of the CBD) essentially disrupted the entire site II interaction between the myosin VI CBD and Dab2 (K_D ~310 nM for the R1152E-CBD/Dab2 MIR complex versus K_D ~420 nM for the wild-type CBD in complex with the αA′ half of the MIR; Figures 2C and 5D), indicating that the charge-charge interactions in site II play critical roles in the binding specificity between myosin VI and Dab2. Most importantly, the interactions in site II play a modulatory role in converting myosin VI from a monomer in its apo-form into a transport-competent dimer upon binding to Dab2 on clathrin-coated vesicles.

The Myosin VI/Dab2 Interaction Is Essential for Myosin VI/Clathrin-Coated Vesicle Colocalization

The role of the interaction between the myosin VI CBD and Dab2 in the localization of the motor on clathrin-coated vesicles was investigated by transiently expressing the wild-type myosin VI tail domain-containing CBD (residues 1040–end) or its L2K, R2E mutants in HeLa cells. As described previously (Buss et al., 2001; Dance et al., 2004; Spudich et al., 2007), the GFP-fused wild-type myosin VI CBD colocalizes well with the clathrin-coated vesicles (Figure 6A1). In contrast, the substitution of L1209 with Lys, which essentially disrupts the interaction between myosin VI and Dab2 (Figure 5), led to a loss of colocalization of the myosin VI CBD to the clathrin-coated vesicles (Figure 6A2), indicating that direct binding between myosin VI and Dab2 is essential for the motor to transport the clathrin-coated vesicles. It is important to note that the R1152E mutant of the myosin VI CBD also did not show any colocalization with the clathrin-coated vesicles (Figure 6A2), even though the mutant CBD binds to Dab2 with reasonably high affinity (K_D ~310 nM, Figure 5D). These data suggest that the Dab2 binding-mediated dimerization of the myosin VI CBD is required for the motor to be colocalized with the clathrin-coated vesicles. Taken together, our data demonstrate that the specific interactions between CBD and Dab2 (seen in both site I and site II) are critical for myosin VI-mediated clathrin-coated vesicle endocytosis.

DISCUSSION

Being the only known minus-ended actin-based molecular motor, myosin VI plays essential roles in a host of cellular functions. Adding complexities to the motor functions, myosin VI is known to exist both in nonprocessive monomer form and processive dimer form in cells. Recent structural and biophysical studies have elucidated the molecular basis governing the

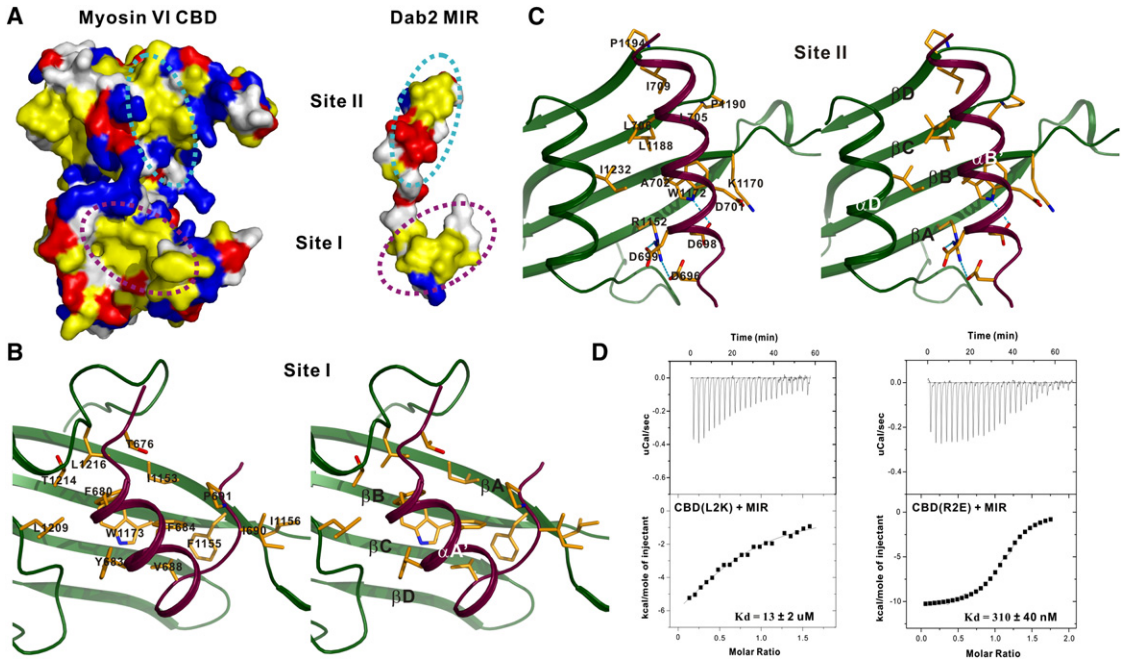

Figure 5. The Details of the Binding between the Myosin VI CBD and the Dab2 MIR

(A) Surface diagram of the myosin VI CBD/Dab2 MIR complex shown in an open-book style. In this presentation, the hydrophobic amino acid residues are drawn in yellow, the positively charged residues in blue, the negatively charged residues in red, and the uncharged polar residues in gray.

(B and C) Detailed molecular interactions between the myosin VI CBD and the Dab2 MIR using the same color scheme as that in Figure 3A.

(D) ITC-based measurements of the interactions between the Dab2 MIR with a "site I" mutant (L1209K) and a "site II" mutant (R1152E) of the myosin VI CBD.

reverse directionality of the motor (Bryant et al., 2007; Menetrey et al., 2005). The most challenging question remaining to be answered for myosin VI is perhaps the molecular mechanism that regulates the monomer-dimer conversion of the motor. The structural studies described here clearly demonstrate that myosin VI undergoes a cargo binding-regulated monomer-to-dimer conversion. Before binding to cargoes (the clathrin-coated vesicle adaptor Dab2 in this case), the myosin VI CBD adopts a stable monomer. Upon binding to Dab2, an extended myosin VI-interaction region of Dab2 tethers myosin VI into a stable dimer. It is interesting to note that the Dab2 MIR exists as an unfolded monomer before binding to the myosin VI CBD. Therefore, the conversion of the myosin VI monomer from its cargo-free form to a Dab2-bound dimer is a result of the synergistic actions of both myosin VI and its cargo, rather than the dimerization of the motor by binding to a pre-existing dimeric adaptor (Figure 6B). It should be noted that the tail domain of myosin VI contains another subdomain (~80 residues) immediately proceeding CBD characterized here, and this subdomain has been shown to bind to lipid membranes as well as other cargoes including GIPC and optineurin (Reed et al., 2005; Sahlender et al., 2005; Spudich et al., 2007). The interaction of this subdomain with lipid membranes would increase the local concentration of the motor and thereby might promote dimerization of myosin VI on the cargo vesicles.

Cargo-mediated dimerization might be a common processivity regulatory mechanism for many molecular motors. For example, myosin VII does not contain the central coiled-coil domain found in known dimeric myosins, and the hypothetical central coiled-coil domain of myosin X was found to form an extended monomeric α helix instead of a coiled-coil dimer (Knight et al., 2005). Yet both myosin VII and myosin X need to form processive dimers for actin-based cargo transport (Knight et al., 2005; Yang et al., 2006). It is possible that both myosin VII and myosin X employ a similar cargo-binding regulated monomer-to-dimer conversion as that of myosin VI, although the detailed molecular mechanisms governing such anticipated conversions remain to be elucidated. The cargo binding-induced dimerization is not limited to actin-based motors. KIF1A/Unc104 has been found to exist as a nonprocessive monomer in solution. Its C-terminal CBD-mediated binding to PI(4,5)P2-containing rafts converts the motor into a processive dimer that is required for vesicle transport (Kikkawa et al., 2000; Klopfenstein et al., 2002; Tomishige et al., 2002). It remains to be established whether certain adaptor protein(s) in addition to PI(4,5)P2 on the vesicles are also required for the KIF1A dimer formation.

The structure of the myosin VI/Dab2 complex determined here reveals that the myosin CBD contains two discrete Dab2-binding sites (sites I and II, Figure 5). The extensive hydrophobic interactions provide the majority of the binding energy for the mysoin VI/Dab2 complex. Interestingly, although the charge-charge interactions in site II only play a minor role in the contribution to the binding energy, these interactions are absolutely required for the Dab2 binding-induced dimer formation of myosin VI. Since charge-charge interactions are generally much more specific than hydrophobic interactions, we speculate that myosin VI (and perhaps other myosin motors) could form either processive dimers or nonprocessive monomers in response to its specific

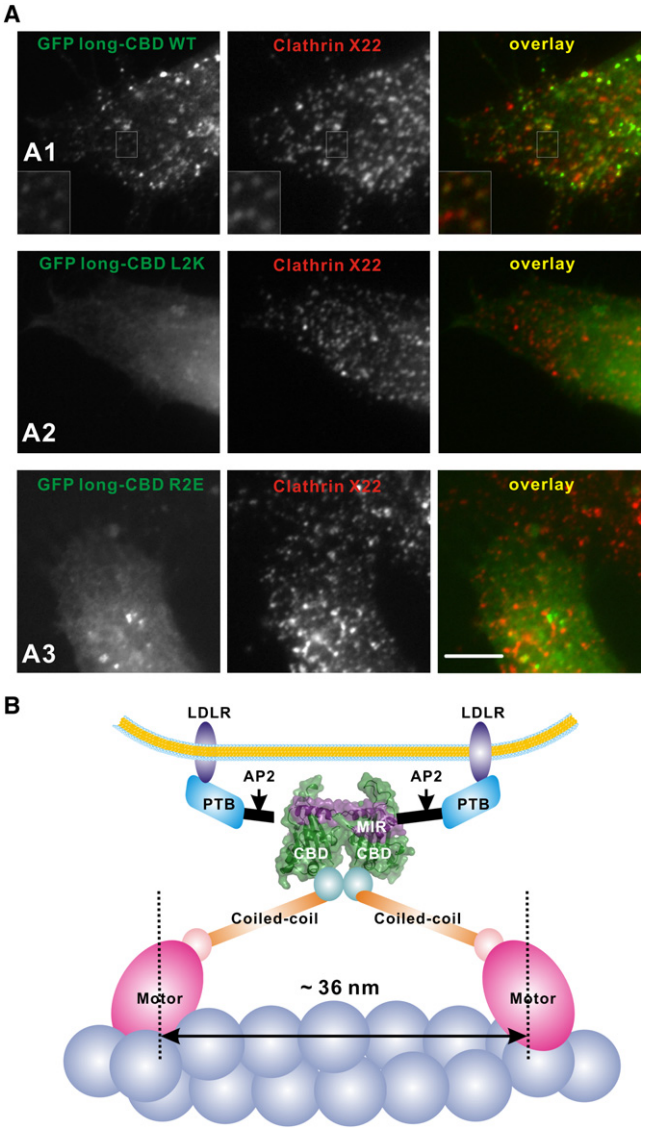

Figure 6. CBD/Dab2 Interaction Is Required for the Colocalization of Myosin VI with Clathrin-Coated Vesicles

(A) Transient expressed GFP-long CBD (i.e., CBD containing an N-terminal extension, residues 1040–end) forms clusters and colocalizes with clathrin-coated vesicles in HeLa cells (A1). Insets highlight the colocalization between the myosin CBD and clathrin-coated vesicles. Disruption of the CBD/Dab2 interaction by substitution of L1209 with Lys ("long-CBD L2K") leads to complete disappearance of the colocalization of the myosin VI CBD with the clathrin-coated vesicles (A2). Disruption of the interaction in site II (R1152E mutation of the CBD) also disrupts the colocalization of the myosin VI CBD with the clathrin-coated vesicles (A3). It is noted that both mutants of the myosin VI CBD are more diffused than the wild-type CBD when expressed in HeLa cells. The scale bar represents 5 μm.

(B) A schematic model showing the Dab2-mediated dimerization of myosin VI during the vesicle/cargo transport. The myosin VI CBD/Dab2 MIR complex is shown in the combined surface and ribbon representations. Other domains of myosin VI and Dab2 are simplified with cartoon representations. The step size between the two heads of myosin VI is ~36 nm. The dimerization of myosin VI is mediated by the synergistic binding between the myosin VI CBD and the Dab2 MIR rather than preformed dimeric cargo adaptors.

cargoes. For example, myosin VI may stay as a nonprocessive monomer if its cargo binding is restricted to site I only. Such monomeric myosin VI/cargo complex formation would be expected to be important for the structural roles of the motor (e.g., connecting cytoskeletons with membranes).

We note with surprise that the interaction between myosin VI and Dab2 is very strong (K_D ~50 nM). Such a strong motor/cargo interaction is somewhat odd, considering the reversible cargo loading and unloading processes required for motor-mediated cargo transport. With such strong binding affinity, it would be difficult for myosin VI-bound Dab2 to dissociate from the motor, given that cellular concentrations of both myosin VI and Dab2 are quite high (Fazili et al., 1999; Hasson and Mooseker, 1994; Rodriguez and Cheney, 2000). It is possible and logically necessary that myosin VI employs some sort of regulatory switch to regulate Dab2-containing cargo loading and unloading. For example, the Dab2 MIR contains several absolutely conserved amino acid residues that can be phosphorylated (e.g., T676, S682, and Y683), and these residues are intimately involved in the interaction with the myosin VI CBD. Based on the structure of the myosin VI/Dab2 complex, the phosphorylation of one or more of these residues would weaken the interaction between the motor and its cargo and thus would facilitate the unloading of the cargo. The identification of such potential phosphorylation-dependent cargo unloading switches of myosin VI represents an important line of future work.

Finally, the elucidation of the interaction mechanism between myosin VI and Dab2 represents a good example of combining two major structural biology techniques, namely NMR spectroscopy and X-ray crystallography, in tackling challenging biological questions. We believe that the combined efforts of NMR spectroscopy and X-ray crystallography can play a larger role in answering challenging biological questions.

EXPERIMENTAL PROCEDURES

Protein Expression and Purification

The mouse myosin VI CBD (residue 1137–end) fused with His_6-tag was expressed in *E. coli* BL21 (DE3) in its native form. The fusion protein was purified by Ni^{2+}-NTA affinity chromatography. After removing His_6-tag, protein was further purified by size-exclusion chromatography. The NMR samples were concentrated to ~0.2 mM (for sample condition screening and titration experiments) or ~1 mM (for structural determinations) in 100 mM sodium phosphate (pH 6.5), 2 mM DTT, and 2 mM EDTA. All point mutants of the myosin VI CBD described in this study were prepared using PCR-based methods and purified using essentially the same method as used for the wild-type protein. The rat Dab2 MIR (residues 675–713) and the MIR αA′ (residues 675–695) (both fused with GB1-tag) were expressed in *E. coli* BL21 (DE3) and purified by Ni^{2+}-NTA affinity chromatography followed by size-exclusion chromatography. For the complex structure determination, the Dab2 MIR was fused to either the N or C terminus of the myosin VI CBD with different lengths of flexible (GS)-linkers coupled with a thrombin cleavage site ("LVPRGS") in the middle. The myosin VI CBD/Dab2 MIR complex proteins were purified using the same procedure for the myosin VI CBD, and the flexible linker was cleaved by thrombin. The protease in the digestion mixture was removed by another step of gel-filtration chromatography.

NMR Spectroscopy and Structure Calculations

NMR spectra were acquired at 30°C on Varian Inova 500 or 750 MHz spectrometers each equipped with a *z*-axis shielded triple resonance probehead. Backbone and nonaromatic, nonexchangeable side chain resonance

assignments of myosin VI L2K-CBD were achieved by standard heteronuclear correlation experiments using $^{15}N/^{13}C$-labeled samples and confirmed by a 3D ^{15}N-separated NOESY experiment using ^{15}N-labeled samples (Bax and Grzesiek, 1993; Kay and Gardner, 1997). The side chains of aromatics were assigned by ^{1}H 2D NMR experiments using unlabeled samples in D_2O (Wuthrich, 1986). Approximate inter-proton distance restraints were derived from 2D ^{1}H-NOESY, 3D ^{15}N-seperated NOESY, and 3D ^{13}C-seperated NOESY spectra. Hydrogen bonding and backbone dihedral angle restraints were generated as described in our earlier work (Feng et al., 2004). Structures were calculated using the program CNS (Brunger et al., 1998).

Crystallography

Crystals of the myosin VI CBD/Dab2 MIR complex were obtained by the hanging drop vapor diffusion method at 16°C. To set up a hanging drop, 1 μl of concentrated protein solution was mixed with 1 μl of crystallization solution with 20% PEG3350, 0.2 M potassium thiocyanate, or 0.2 M sodium iodide (pH 7.0) buffer. Before X-ray diffraction, crystals were soaked in crystallization solution containing 20% glycerol for cryoprotection. The diffraction data of native and iodine derivative crystals were collected at 100 K on a Rigaku RAXIS IV++ imaging-plate system with a MicroMax-007 copper rotating-anode generator. The data were processed and scaled using the MOSFLM and SCALA in the CCP4 suite (CCP4, 1994). We failed to solve the complex structure by the molecular replacement method using the NMR structure of myosin VI L2K-CBD as the search model. The NaI data set was then used for heavy atom substructure determination. Four iodine sites were found by SHELXD (Sheldrick, 2008). The site refinement and phase improvement were carried out by autoSHARP (Vonrhein et al., 2007). The program Molrep (Vagin and Teplyakov, 2000) was then employed for searching the CBD model derived from the NMR structure in the density map. After four CBD models were located, the backbone was rebuilt manually based on the density map to produce an initial model. With the combination of phase information from the initial model, the phase was further improved by RESOLVE (Terwilliger, 2000) and used as the input for ARP/wARP model building (Perrakis et al., 1999). The output model was refined in Refmac5 (Vagin et al., 2004) against the 2.2 Å native data set. COOT was used for model rebuilding and adjustments (Emsley and Cowtan, 2004).

Isothermal Titration Calorimetry Assay

Isothermal titration calorimetry (ITC) measurements were carried out on a VP-ITC Microcal calorimeter (Microcal) at 25°C. All protein samples were in 50 mM (pH 6.5) phosphate buffer. The titration processes were performed by injecting 5–10 μl aliquots of the myosin VI CBD into Dab2 proteins (or GB1 as the control) at time intervals of 2 min to ensure that the titration peak returned to the baseline. The titration data were analyzed using the program Origin7.0 and fitted by the one-site binding model.

Disufide-Mediated Chemical Crosslinking

Myosin VI CBD(L1225C) and the myosin VI CBD(L1225C)/Dab2 MIR complex were purified using the method described for the wild-type CBD counterparts. The Dab2 MIR αA′ peptide was directly added into the myosin VI CBD(L1225C) to make the myosin VI CBD(L1225C)/Dab2 MIR αA′ peptide complex. To initiate chemical crosslinking, DTT was removed from the protein samples by gel filtration and the samples were left at room temperature with or without addition of $[Cu(Phen)3]^{2+}$ ($[Cu(1,10\text{-phenanthroline})_3]^{2+}$ (0.75 mM final concentration) for 20 min. The concentration of the proteins used in the assay was 25 μM. All the samples were mixed with SDS loading buffer without or with 10 mM DTT at final concentration and analyzed by SDS-PAGE.

Cell Culture and Imaging

The globular tail domain of myosin VI containing CBD (residues 1040–end) and its mutants were individually cloned into a modified pEGFP-C3 vector (Invitrogen). HeLa cells were transfected with 0.5 μg of each form of CBD plasmids per well using the Lipofetamine Plus transfection kit (Invitrogen) and were subsequently cultured for ~24 hr before fixation by 4% paraformaldehyde (PFA) and permeabilization with 0.2% Triton X-100 in PBS. After washing with PBS, cells were incubated with primary (mouse monoclonal antibody X22 to clathrin, abcam) and rhodamine red X-conjugated secondary antibody (anti-mouse, Jackson's Laboratory). The images were acquired on a Nikon TE2000E inverted fluorescent microscope.

Illustrations

The protein structure figures were prepared using the programs MOLMOL (Koradi et al., 1996), MOLSCRIPT (Kraulis, 1991), PyMOL (http://pymol.sourceforge.net/), and GRASP (Nicholls, 1992).

ACCESSION NUMBERS

The atomic coordinates of the myosin VI L2K-CBD and the myosin VI CBD in complex with the Dab2 MIR have been deposited in the Protein Data Bank under ID codes 2KIA and 3H8D, respectively.

SUPPLEMENTAL DATA

Supplemental Data include six figures and one table and can be found with this article online at http://www.cell.com/supplemental/S0092-8674(09)00633-3.

ACKNOWLEDGMENTS

We thank Anthony Zhang for critical reading of the manuscript and Joanne Chan for technical help. This work was supported by grants from the Research Grants Council of Hong Kong to M.Z. (HKUST6419/05M, 6442/06M, 663407, 663808, CA07/08.SC01, and AoE/B-15/01-II), W.F. (660708), and Y.Z. (PolyU5641/08M). The NMR spectrometers used in this work were purchased with funds donated to the Biotechnology Research Institute by the Hong Kong Jockey Club.

Received: February 9, 2009
Revised: April 2, 2009
Accepted: May 6, 2009
Published: August 6, 2009

REFERENCES

Altman, D., Goswami, D., Hasson, T., Spudich, J.A., and Mayor, S. (2007). Precise positioning of myosin VI on endocytic vesicles in vivo. PLoS Biol. *5*, e210. 10.1371/journal.pbio.0050210.

Aschenbrenner, L., Lee, T., and Hasson, T. (2003). Myo6 facilitates the translocation of endocytic vesicles from cell peripheries. Mol. Biol. Cell *14*, 2728–2743.

Au, J.S., Puri, C., Ihrke, G., Kendrick-Jones, J., and Buss, F. (2007). Myosin VI is required for sorting of AP-1B-dependent cargo to the basolateral domain in polarized MDCK cells. J. Cell Biol. *177*, 103–114.

Baker, J.P., and Titus, M.A. (1997). A family of unconventional myosins from the nematode Caenorhabditis elegans. J. Mol. Biol. *272*, 523–535.

Bax, A., and Grzesiek, S. (1993). Methodological advaces in protein NMR. Acc. Chem. Res. *26*, 131–138.

Brunger, A.T., Adams, P.D., Clore, G.M., DeLano, W.L., Gros, P., Grosse-Kunstleve, R.W., Jiang, J.S., Kuszewski, J., Nilges, M., Pannu, N.S., et al. (1998). Crystallography & NMR system: A new software suite for macromolecular structure determination. Acta Crystallogr. D Biol. Crystallogr. *54*, 905–921.

Bryant, Z., Altman, D., and Spudich, J.A. (2007). The power stroke of myosin VI and the basis of reverse directionality. Proc. Natl. Acad. Sci. USA *104*, 772–777.

Bunn, R.C., Jensen, M.A., and Reed, B.C. (1999). Protein interactions with the glucose transporter binding protein GLUT1CBP that provide a link between GLUT1 and the cytoskeleton. Mol. Biol. Cell *10*, 819–832.

Buss, F., and Kendrick-Jones, J. (2008). How are the cellular functions of myosin VI regulated within the cell? Biochem. Biophys. Res. Commun. *369*, 165–175.

Buss, F., Arden, S.D., Lindsay, M., Luzio, J.P., and Kendrick-Jones, J. (2001). Myosin VI isoform localized to clathrin-coated vesicles with a role in clathrin-mediated endocytosis. EMBO J. *20*, 3676–3684.

Buss, F., Spudich, G., and Kendrick-Jones, J. (2004). Myosin VI: cellular functions and motor properties. Annu. Rev. Cell Dev. Biol. *20*, 649–676.

CCP4 (Collaborative Computational Project, Number 4). (1994). The CCP4 suite: programs for protein crystallography. Acta Crystallogr. D Biol. Crystallogr. *50*, 760–763.

Dance, A.L., Miller, M., Seragaki, S., Aryal, P., White, B., Aschenbrenner, L., and Hasson, T. (2004). Regulation of myosin-VI targeting to endocytic compartments. Traffic *5*, 798–813.

Emsley, P., and Cowtan, K. (2004). Coot: model-building tools for molecular graphics. Acta Crystallogr. D Biol. Crystallogr. *60*, 2126–2132.

Fazili, Z., Sun, W., Mittelstaedt, S., Cohen, C., and Xu, X.X. (1999). Disabled-2 inactivation is an early step in ovarian tumorigenicity. Oncogene *18*, 3104–3113.

Feng, W., Long, J.F., Fan, J.S., Suetake, T., and Zhang, M. (2004). The tetrameric L27 domain complex as an organization platform for supramolecular assemblies. Nat. Struct. Mol. Biol. *11*, 475–480.

Foth, B.J., Goedecke, M.C., and Soldati, D. (2006). New insights into myosin evolution and classification. Proc. Natl. Acad. Sci. USA *103*, 3681–3686.

Geisbrecht, E.R., and Montell, D.J. (2002). Myosin VI is required for E-cadherin-mediated border cell migration. Nat. Cell Biol. *4*, 616–620.

Hasson, T., and Mooseker, M.S. (1994). Porcine myosin-VI: characterization of a new mammalian unconventional myosin. J. Cell Biol. *127*, 425–440.

Hasson, T., Skowron, J.F., Gilbert, D.J., Avraham, K.B., Perry, W.L., Bement, W.M., Anderson, B.L., Sherr, E.H., Chen, Z.Y., Greene, L.A., et al. (1996). Mapping of unconventional myosins in mouse and human. Genomics *36*, 431–439.

Hasson, T., Gillespie, P.G., Garcia, J.A., MacDonald, R.B., Zhao, Y., Yee, A.G., Mooseker, M.S., and Corey, D.P. (1997). Unconventional myosins in inner-ear sensory epithelia. J. Cell Biol. *137*, 1287–1307.

Inoue, A., Sato, O., Homma, K., and Ikebe, M. (2002). DOC-2/DAB2 is the binding partner of myosin VI. Biochem. Biophys. Res. Commun. *292*, 300–307.

Kay, L.E., and Gardner, K.H. (1997). Solution NMR spectroscopy beyond 25 kDa. Curr. Opin. Struct. Biol. *7*, 722–731.

Kellerman, K.A., and Miller, K.G. (1992). An unconventional myosin heavy chain gene from Drosophila melanogaster. J. Cell Biol. *119*, 823–834.

Kikkawa, M., Okada, Y., and Hirokawa, N. (2000). 15 A resolution model of the monomeric kinesin motor, KIF1A. Cell *100*, 241–252.

Klopfenstein, D.R., Tomishige, M., Stuurman, N., and Vale, R.D. (2002). Role of phosphatidylinositol(4,5)bisphosphate organization in membrane transport by the Unc104 kinesin motor. Cell *109*, 347–358.

Knight, P.J., Thirumurugan, K., Xu, Y., Wang, F., Kalverda, A.P., Stafford, W.F., 3rd, Sellers, J.R., and Peckham, M. (2005). The predicted coiled-coil domain of myosin 10 forms a novel elongated domain that lengthens the head. J. Biol. Chem. *280*, 34702–34708.

Koradi, R., Billeter, M., and Wuthrich, K. (1996). MOLMOL: a program for display and analysis of macromolecular structures. J. Mol. Graph. *14*, 51–55, 29–32.

Kraulis, P.L. (1991). MOLSCRIPT: a program to produce both detailed and schematic plots of protein structures. J. Appl. Cryst. *24*, 946–950.

Lister, I., Schmitz, S., Walker, M., Trinick, J., Buss, F., Veigel, C., and Kendrick-Jones, J. (2004). A monomeric myosin VI with a large working stroke. EMBO J. *23*, 1729–1738.

Maddugoda, M.P., Crampton, M.S., Shewan, A.M., and Yap, A.S. (2007). Myosin VI and vinculin cooperate during the morphogenesis of cadherin cell cell contacts in mammalian epithelial cells. J. Cell Biol. *178*, 529–540.

Menetrey, J., Bahloul, A., Wells, A.L., Yengo, C.M., Morris, C.A., Sweeney, H.L., and Houdusse, A. (2005). The structure of the myosin VI motor reveals the mechanism of directionality reversal. Nature *435*, 779–785.

Menetrey, J., Llinas, P., Mukherjea, M., Sweeney, H.L., and Houdusse, A. (2007). The structural basis for the large powerstroke of myosin VI. Cell *131*, 300–308.

Menetrey, J., Llinas, P., Cicolari, J., Squires, G., Liu, X., Li, A., Sweeney, H.L., and Houdusse, A. (2008). The post-rigor structure of myosin VI and implications for the recovery stroke. EMBO J. *27*, 244–252.

Mermall, V., McNally, J.G., and Miller, K.G. (1994). Transport of cytoplasmic particles catalysed by an unconventional myosin in living Drosophila embryos. Nature *369*, 560–562.

Mishra, S.K., Keyel, P.A., Hawryluk, M.J., Agostinelli, N.R., Watkins, S.C., and Traub, L.M. (2002). Disabled-2 exhibits the properties of a cargo-selective endocytic clathrin adaptor. EMBO J. *21*, 4915–4926.

Morris, S.M., and Cooper, J.A. (2001). Disabled-2 colocalizes with the LDLR in clathrin-coated pits and interacts with AP-2. Traffic *2*, 111–123.

Morris, S.M., Arden, S.D., Roberts, R.C., Kendrick-Jones, J., Cooper, J.A., Luzio, J.P., and Buss, F. (2002). Myosin VI binds to and localises with Dab2, potentially linking receptor-mediated endocytosis and the actin cytoskeleton. Traffic *3*, 331–341.

Naccache, S.N., Hasson, T., and Horowitz, A. (2006). Binding of internalized receptors to the PDZ domain of GIPC/synectin recruits myosin VI to endocytic vesicles. Proc. Natl. Acad. Sci. USA *103*, 12735–12740.

Nicholls, A. (1992). GRASP: graphical representation and analysis of surface properties (New York: Columbia University).

O'Connell, C.B., Tyska, M.J., and Mooseker, M.S. (2007). Myosin at work: motor adaptations for a variety of cellular functions. Biochim. Biophys. Acta *1773*, 615–630.

Park, H., Ramamurthy, B., Travaglia, M., Safer, D., Chen, L.Q., Franzini-Armstrong, C., Selvin, P.R., and Sweeney, H.L. (2006). Full-length myosin VI dimerizes and moves processively along actin filaments upon monomer clustering. Mol. Cell *21*, 331–336.

Perrakis, A., Morris, R., and Lamzin, V.S. (1999). Automated protein model building combined with iterative structure refinement. Nat. Struct. Biol. *6*, 458–463.

Reed, B.C., Cefalu, C., Bellaire, B.H., Cardelli, J.A., Louis, T., Salamon, J., Bloecher, M.A., and Bunn, R.C. (2005). GLUT1CBP(TIP2/GIPC1) interactions with GLUT1 and myosin VI: evidence supporting an adapter function for GLUT1CBP. Mol. Biol. Cell *16*, 4183–4201.

Rock, R.S., Rice, S.E., Wells, A.L., Purcell, T.J., Spudich, J.A., and Sweeney, H.L. (2001). Myosin VI is a processive motor with a large step size. Proc. Natl. Acad. Sci. USA *98*, 13655–13659.

Rodriguez, O.C., and Cheney, R.E. (2000). A new direction for myosin. Trends Cell Biol. *10*, 307–311.

Sahlender, D.A., Roberts, R.C., Arden, S.D., Spudich, G., Taylor, M.J., Luzio, J.P., Kendrick-Jones, J., and Buss, F. (2005). Optineurin links myosin VI to the Golgi complex and is involved in Golgi organization and exocytosis. J. Cell Biol. *169*, 285–295.

Seiler, C., Ben-David, O., Sidi, S., Hendrich, O., Rusch, A., Burnside, B., Avraham, K.B., and Nicolson, T. (2004). Myosin VI is required for structural integrity of the apical surface of sensory hair cells in zebrafish. Dev. Biol. *272*, 328–338.

Sellers, J.R. (2000). Myosins: a diverse superfamily. Biochim. Biophys. Acta *1496*, 3–22.

Sheldrick, G.M. (2008). A short history of SHELX. Acta Crystallogr. A *64*, 112–122.

Spink, B.J., Sivaramakrishnan, S., Lipfert, J., Doniach, S., and Spudich, J.A. (2008). Long single α-helical tail domains bridge the gap between structure and function of myosin VI. Nat. Struct. Mol. Biol. *15*, 591–597.

Spudich, G., Chibalina, M.V., Au, J.S., Arden, S.D., Buss, F., and Kendrick-Jones, J. (2007). Myosin VI targeting to clathrin-coated structures and dimerization is mediated by binding to Disabled-2 and PtdIns(4,5)P2. Nat. Cell Biol. *9*, 176–183.

Sweeney, H.L., and Houdusse, A. (2007). What can myosin VI do in cells? Curr. Opin. Cell Biol. *19*, 57–66.

Terwilliger, T.C. (2000). Maximum-likelihood density modification. Acta Crystallogr. D Biol. Crystallogr. *56*, 965–972.

Tomishige, M., Klopfenstein, D.R., and Vale, R.D. (2002). Conversion of Unc104/KIF1A kinesin into a processive motor after dimerization. Science *297*, 2263–2267.

Vagin, A., and Teplyakov, A. (2000). An approach to multi-copy search in molecular replacement. Acta Crystallogr. D Biol. Crystallogr. *56*, 1622–1624.

Vagin, A.A., Steiner, R.A., Lebedev, A.A., Potterton, L., McNicholas, S., Long, F., and Murshudov, G.N. (2004). REFMAC5 dictionary: organization of prior chemical knowledge and guidelines for its use. Acta Crystallogr. D Biol. Crystallogr. *60*, 2184–2195.

Vonrhein, C., Blanc, E., Roversi, P., and Bricogne, G. (2007). Automated structure solution with autoSHARP. Methods Mol. Biol. *364*, 215–230.

Wells, A.L., Lin, A.W., Chen, L.Q., Safer, D., Cain, S.M., Hasson, T., Carragher, B.O., Milligan, R.A., and Sweeney, H.L. (1999). Myosin VI is an actin-based motor that moves backwards. Nature *401*, 505–508.

Wu, H., Nash, J.E., Zamorano, P., and Garner, C.C. (2002). Interaction of SAP97 with Minus-end-directed actin motor myosin VI. Implication for AMPA receptor trafficking. J. Biol. Chem. *277*, 30928–30934.

Wuthrich, K. (1986). NMR of Proteins and Nucleic Acids (New York: John Wiley & Sons, Inc.).

Yang, Y., Kovacs, M., Sakamoto, T., Zhang, F., Kiehart, D.P., and Sellers, J.R. (2006). Dimerized Drosophila myosin VIIa: a processive motor. Proc. Natl. Acad. Sci. USA *103*, 5746–5751.